Vietnam Journal of Earth Sciences, 43(1), 33-56, https://doi.org/10.15625/0866-7187/15694

Vietnam Academy of Science and Technology
Vietnam Journal of Earth Sciences
http://www.vjs.ac.vn/index.php/jse

Pliocene - present tectonics and strain rate in Ninh Thuan region and surrounding continental shelf

Ngo Van Liem[1], Phan Trong Trinh[*2,5,6], Tran Van Phong[2], Vy Thi Hong Lien[2], Nguyen Van Huong[1], Nguyen Quang Xuyen[2], Bui Nhi Thanh[3,5], Duong Van Hao[4], Binh Thai Pham[7], Nguyen Van Dung[8], Vu Khac Dang[9], Vu Hoa An[10]

[1]*VNU University of Science, Vietnam National University, Hanoi, Vietnam*
[2]*Institute of Geological Sciences, VAST, Hanoi, Vietnam*
[3]*Institute of Marine Geology and Geophysics, VAST, Hanoi, Vietnam*
[4]*Hanoi University of Mining and Geology, Hanoi, Vietnam*
[5]*Graduate University of Science and Technology, VAST, Hanoi, Vietnam*
[6]*Royal Academy for Overseas Sciences, Brussels, Belgium*
[7]*University of Transport Technology, Hanoi, Vietnam*
[8]*Institute of Geography, VAST, Hanoi, Vietnam*
[9]*Department of Geography, Hanoi National University of Education, Hanoi, Vietnam*
[10]*Institute of Geophysics, VAST, Hanoi, Vietnam*

Received 10 July 2020; Received in revised form 16 October 2020; Accepted 1 December 2020

ABSTRACT

In this paper, we present detail data of Pliocene - present tectonics and strain rate from GPS measurement and seismic interpretation. Using international reference frame ITRF08, we revealed absolute tectonic velocities of GPS sites with the slip rate to the east between 22 to 25 mm/year, to the south between 4 to 8 mm/year. The present strain rate was determined from present tectonic velocities that were consistent with the recent strain rates determined from seismic profiles, thickness of Pliocene - Quaternary sediments. Present day strain rate varying from 10 to 30 nano per year indicated that the region has been deformed weakly, in a stable tectonic regime.

Keywords: Present day tectonics, GPS, strain rate, tectonic gradient, seismic profiles, continental shelf.

1. Introduction

In coastal areas, many constructions such as seaports, roads, telecommunications, petroleum industry, and major projects such as nuclear power plants have been built. In strong tectonic areas, the ability to recur earthquakes is from hundreds to thousands of years. In the weaker tectonic area, the repeated earthquake cycle is considered much longer from Quaternary up to the present (Huong et al., 2020). Research on contemporary tectonic and strain rate will not only reveal the possibility of earthquake recurrence but also the source of seismic activity in the area (Huong et al., 2020). The slow capable faults are not visible on the land or covered by young formations. However, analysis of the tectonic gradient or strain rate

*Corresponding author, Email: phantrongt@yahoo.com

can reveal these faults. This paper has the aim of presenting in detail the Pliocene tectonic and strain rate in Ninh Thuan and surrounding areas for the construction of important works in the coastal area. We based on remote sensing, fault observation, seismic profile analysis, and GPS measurement to detect contemporary tectonics and strain rate in Ninh Thuan and surrounding areas.

2. Tectonic setting

Ninh Thuan area is located in the south of Indochina block with a long tectonic history (Fig. 1). The collision of India to Asia caused the thickening of the crust underneath the Tibetan Plateau and the extrusion of the Indochinese block to the southeast. Clockwise rotation of the Indochinese block happened along major faults like the Mae Ping Fault, the Sagaing Fault, and the Red River Fault (Tapponnier et al., 1982). The continuation of the Red River fault crosses the seabed off the coast of Vietnam and even Borneo (Leloup et al., 1995; 2001). In the extrusion model (Tapponnier et al., 1986), the opening of the East Vietnam Sea took place between 16 and 32 million years (Thanh et al., 2018). However, in the Pull-slab model, the presence of an old subduction zone below northwest Borneo can have a slab drag effect and may also explain the spread of the East Vietnam Sea (Taylor and Hayes, 1980). After 16 Ma, the clockwise rotation of the Indochinese block and the left movement on the Red River fault terminates, leading to the spread along the East Vietnam Sea to cease, when the Indian indentation passed through Indochina (Peltzer and Tapponnier, 1988; Leloup et al.; 1995; 2001; Tapponnier et al., 1982). From Pliocene to the present, the Red River fault movement is right-lateral strike-slip, with a velocity of 5 mm/year or several mm/yr in late Quaternary that is the seismic source in the region (Replumaz et al., 2001; Trinh et al., 2012; Nhung et al., 2018; Huong et al., 2018; Hoan et al., 2018). The change in the regional tectonic stress model caused by India's regression to Eurasia and the rift off Central Vietnam caused the dominance of the right-lateral strike-slip fault in the Indochinese block (Huchon et al., 1994). Both phases of the collision caused crust expansion in central and southern Indochina and caused the modern Neogen-volcano (Rangin et al., 1995; Huong et al., 2018; Phuc et al., 2018).

The brittle tectonic analysis shows two main stages of tectonic stress control in Indochina, including Central South Vietnam in Cenozoic (Trinh et al., 2013; Huong et al., 2011; Binh et al., 2011). The first phase with the maximum east-west compression axis occurred before Pliocene, which is compatible with the left lateral strike-slip along the Red River fault as well as the spread periods in the East Vietnam Sea from 32 to 17 million years. In the second stage, the stress field has a north-south axis of compression formed from Pliocene, which is related to the tectonic features of Vietnam as right-lateral slip along the Red River fault and the NW-SE fault system (Findlay, 2018). The present-day geodynamics of Southeast Asia has been demonstrated through local and regional GPS observations made in the 1990s (Tregoning et al., 1994). GPS network in SE Asia indicates that the core of the Indochina block belonging to the hardware of the Sundaland sub-segment moves to Southeast compared to Eurasia (Michel et al., 2000; 2001). A geodetic network across the Red River fault shows that the maximum slip rate along the fault zone is less than 0.3 μrad/year Cong & Feigl (1999). Based on data from the GPS campaign from 1994 to 200, Feigl et al. (2003) concluded that the shear rate of the Red River fault was less than 2 mm/year. Moreover, there is no significant difference in tectonic movement between Sunda and South China blocks (Michel et al., 2001; Iwakuni et al., 2004).

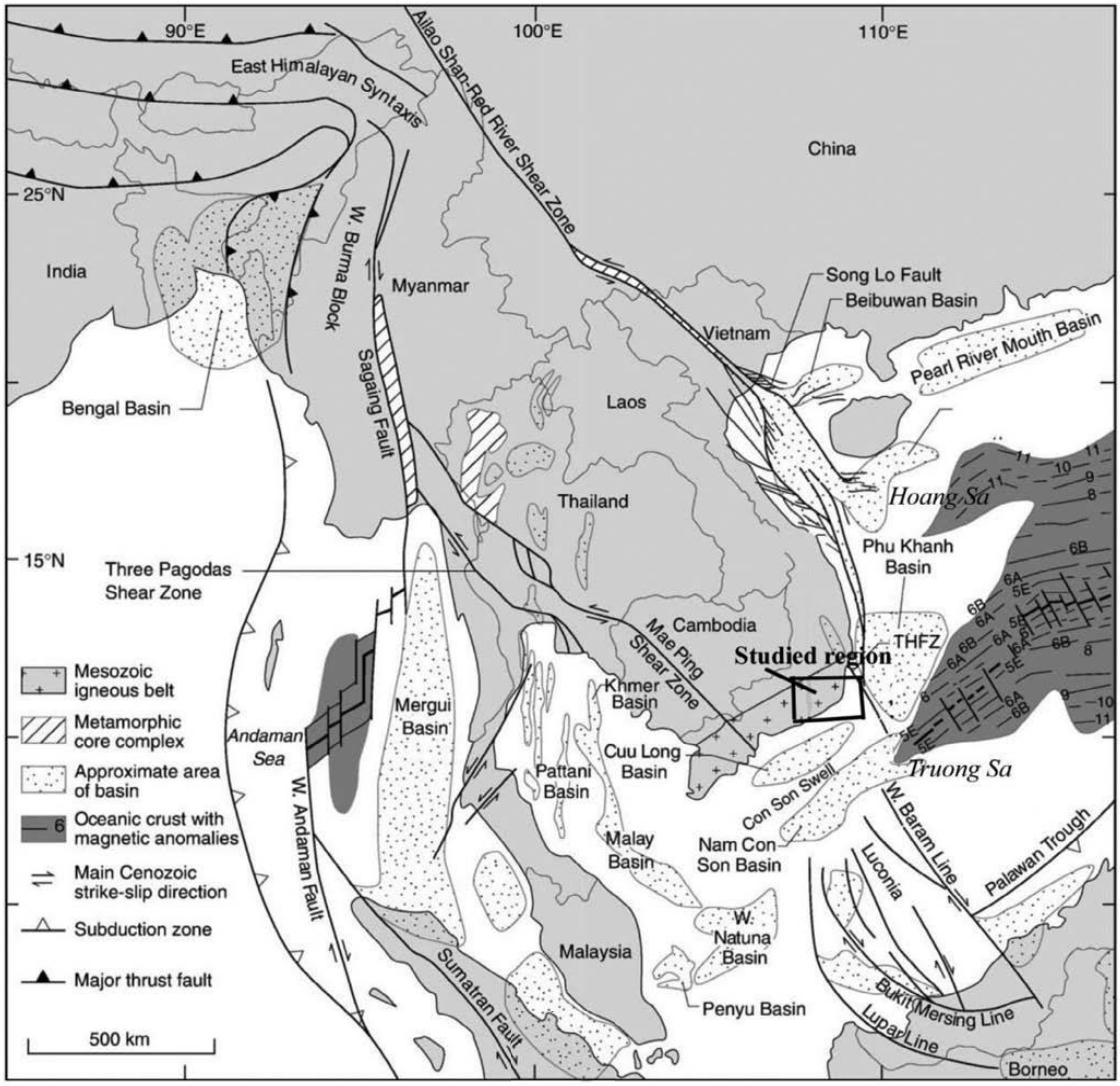

Figure 1. Studied region (modified from Fyhn et al., 2009)

3. Data and methods

Seismic reflection profiles were used from Petro Vietnam, and Japan Atomic Power Company. Drilling cores were used from JAPC and Energy project Technology (Russian consular).

3.1. Geological investigations

Remote sensing and geomorphological observations show that the processes and geomorphology are controlled by tectonic activities. We focus on fracture - geomorphology related to recent faults. Cataclasite and fault gouge exhibit brittle deformation at low temperatures. Distortions near the ground, indicated by cataclasite, fragments of mineral particles with the particles rotated and slipped and expanded. The fine grain of a crack near the surface is essentially a powder formed during fracture. Brittle fracture zones in the rock bed consist of a primary shear plane delimited by a fault zone.

3.2 Seismic reflection profiles

Interpretation of seismic reflections involves matching reflections in 2D or 3D data sets and using them as the basis for geological interpretation. The interpretation of the seismic profile allows for mapping the spatial transformation of strata layers. We use these maps to determine sediment thickness and to identify patterns of sediment layers. There are many solutions in the analysis of seismic cross-section with a data set, so one needs to use more data to find the optimal solution. It is especially important to compare the seismic cross-section with the borehole measurements. In our study, the most concern is signs of the existence of capable faults and Pliocene sediment thickness.

3.3. GPS Analysis

The BERNESE software is one of the highest precision software for calculation of GPS measurement (Dach R., et al., 2015): (1) This software can process any record of high precision (2) This software can process all frequency data and maximum reduction of the influence of ionosphere. (3) This software can combine GPS with GLONASS. (4) This software can process data in zero difference mode or in double-difference mode. (5) This software uses different combinations of L1 and L2. (6) This software can process baselines/sessions/campaigns/multiple campaigns. (7) This software can combine data from different types of receivers. (8) This software can correct phase ambiguity on a very long baseline. (9) The software can process static and dynamic applications. (10) This software can model the movement of the array, tidal load, (11) This software performs different troposphere mapping functions. (12) This software can correct the high-order ionosphere.

3.4. Strain rate

We perform the calculation of deformation rate based on geomorphological, geological, and GPS data collected in the field and analyzed by calculation programs. Google Earth imagery was used to extract topographic profiles. The profiles were then cross-checked with a topographic map. The levels of the Late Pleistocene shelf are determined during these steps and their age is determined based on the radiocarbon dating of the coral samples collected in the terraces. Then, we calculate the vertical strain rate of the study area based on the height and age of the terrace surface. We calculate the strain rate from the likely error length and the likely slip error. The rate of unspecified slip is determined from the formula of Woodward-Clyde (Woodward-Clyde, 1983). On the sea, we estimate the tectonic gradient based on the change in the thickness of the Pliocene sediment. This value is considered to be in proportion with the strain rate.

The present-day strain rate in the study area is determined from the velocity solution of Ninh Thuan GPS stations. QOCA software was used for calculating the strain rate from the geodetic networks (Dong et al., 1998, Feigl et al., 1993). This software uses the location position, velocity (horizontal displacement), and parameters to calculate simultaneously the 2-D horizontal strain rate and maximum shear strain rate. We set up to calculate the strain for each triangle subnet by the least-squares matching method. Six triangular subnets are identified based on the positions of 7 GPS stations on the Ninh Thuan network. The asymmetry of the triangles will affect the accuracy of the strain calculation. Other strain parameters such as the first variable and the second variable of the strain rate tensor, as well as the rotational strain rate for each triangle, are also reported in the results table. In order to calculate the new current tectonic strain rate field throughout Ninh Thuan and the vicinity, we obtain the constant velocity gradient tension field

through interpolation of the scattered observed velocities. Before interpolation, we transfer GPS data from various reference systems using the Horizontal Time-Dependent Positioning to convert position over time (Pearson & Snay, 2012). Interpolation is performed using larger-scale data sets i.e. aggregate velocity data combined from the surrounding environment, with the usual kriging method at 0.2° × homogeneous mesh nodes. 0.2°. Therefore, strain parameters are then computed for each 0.2° × 0.2° rectangular subnet. The map of the strain model is plotted by meshing unevenly distributed data with continuous curves adjusted using the Common Mapping Tool's surface module (Wessel et al., 2013) with a tension factor of 0.25, a convergence limit of 0.01, and a distance of 1 km between the estimated point.

4. Results

4.1. Capable faults

From remote sensing, we were able to identify fault scarps inland. Our field study showed the occurrence of the fault along the F1 fault (Huong et al., 2020). JAPC made trenches across on the F2 fault scarp. The trenching survey showed no faults, deformation, and displacement of the sediments above the foundation rock layers. The JAPC considers the F3 fault scarp to be a capable fault. We observed the displacement along these faults was low with the trace of small tectonic clay. We noticed there is no evidence of deformation of sediments above foundation rocks. We have arguments that point to the F4 fault scarp as a capable fault, sliding left lateral strike-slip with the normal component. Acoustic stratigraphy of neighboring waters is separated from Unit A to Unit E (Huong et al., 2020). Figure 2 shows a comparison between the 15-G-1X borehole in the Cuu Long basin in the south and the seismic cross-section (Fyhn et al., 2009). The classification of layers is done by comparing the seismic cross-section and strata in the borehole.

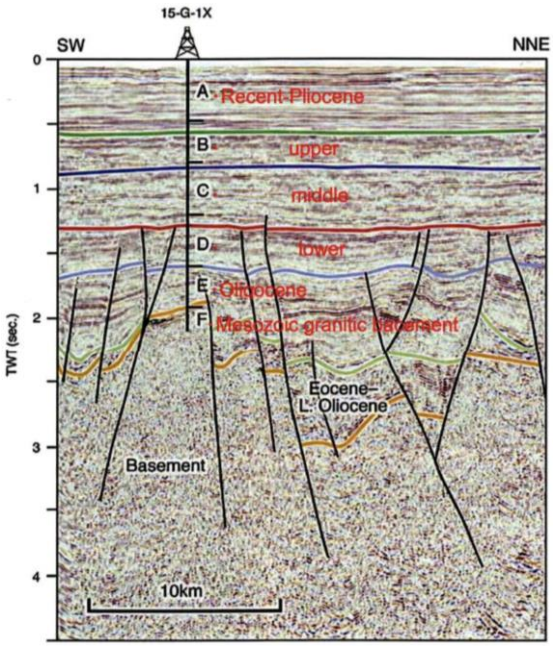

Figure 2. Seismic profile compared with stratigraphic classification in drilling core (Fyhn et al., 2009)

Sediment age in shallow seabed areas provided by the General Department of Sea and Islands. Comparing the drill core taken near the coast of Cam Ranh Bay including a high-resolution shallow seismic cross-section using a boom device, JAPC determined the top layer (Huong et al., 2020).

We have presented here evidence of a number of capable faults that can occur offshore. Capable faults will be mapped if we observe the displacement in Late Pliocene or the fault cuts the sediments from B4. Offshore we can provide evidence of capable faults from the end of the Pliocene (Figs. 3, 4). The map of capable faults in Ninh Thuan and the surrounding region is represented in Fig. 5.

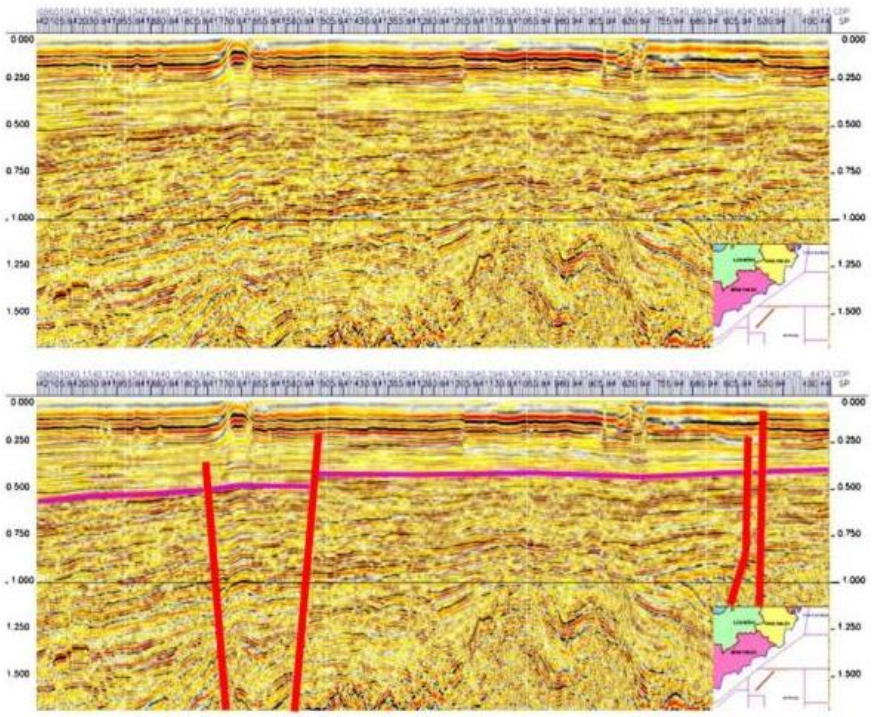

Figure 3. Evidence of capable fault investigated along seismic profile CV910202a-202b (data from Petro Vietnam, interpretation of this study)

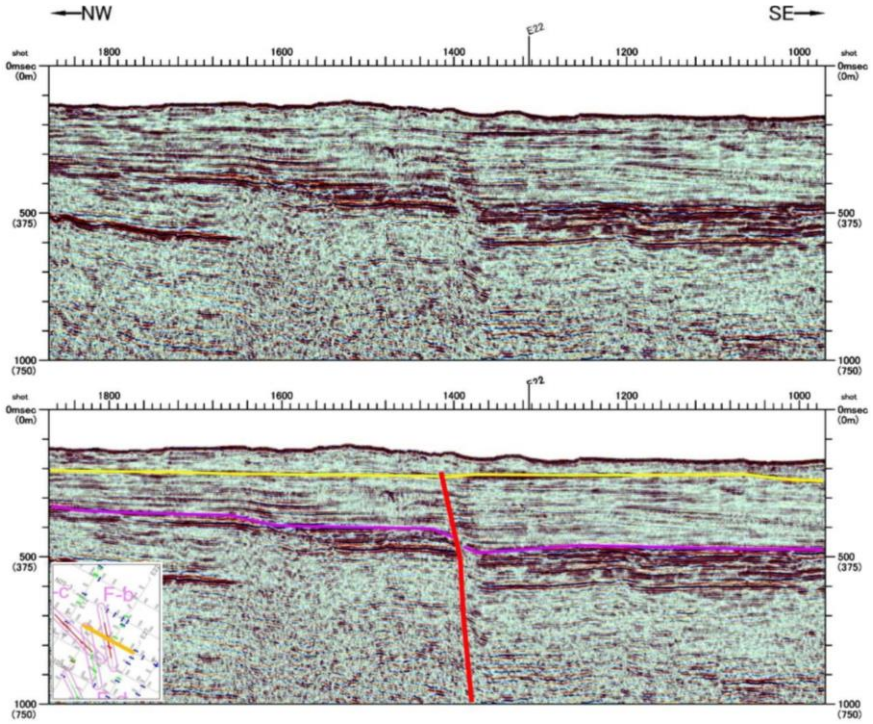

Figure 4. Evidence of normal strike-slip capable fault activated in late Pliocene and Pleistocene along seismic profile (data from JAPC and EVN, interpretation of this study)

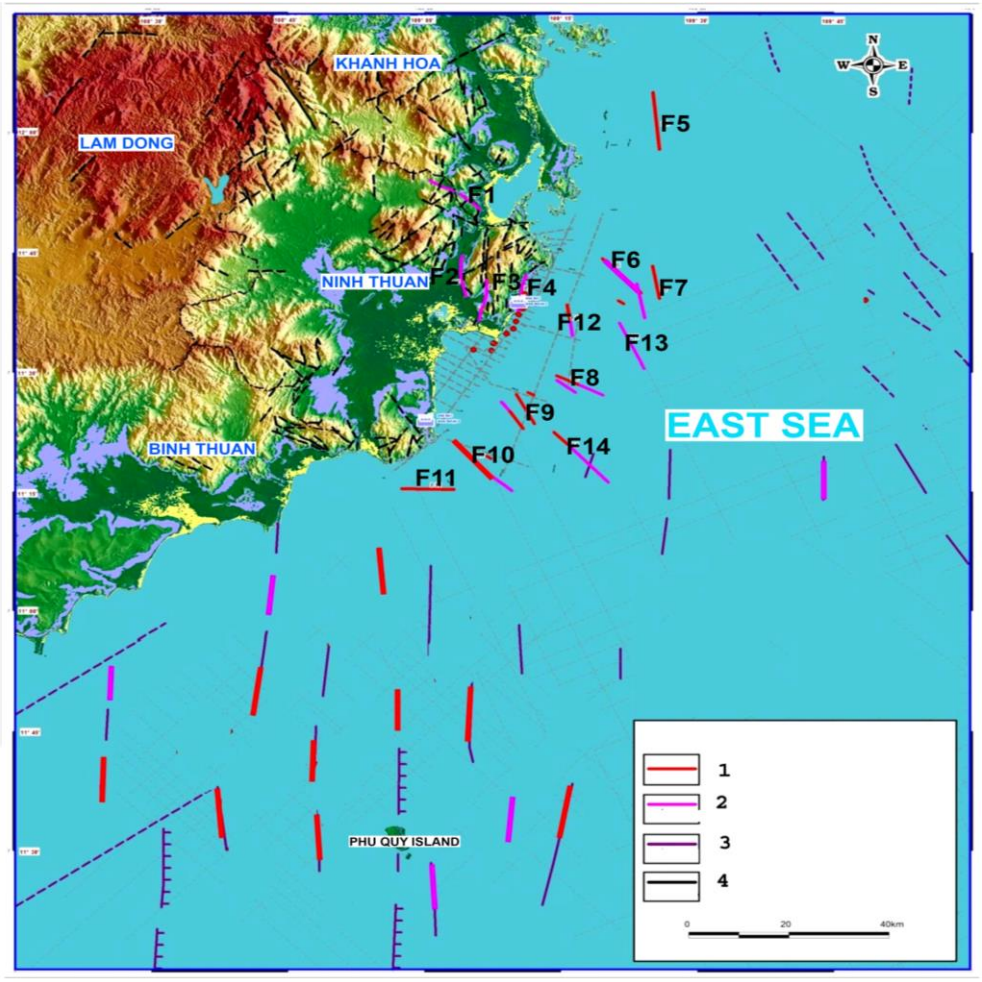

Figure 5. The distribution of capable faults in Ninh Thuan and surrounding regions

4.2. Velocities of present day tectonics

Three campaigns of GPS measurement were effected in 2012-2013. TRIMBLE SSI COMPACT L1/L2 receiver was used to record signals. 7-day data was collected and the logging time for each day was 23 hours 40 minutes at each campaign. Using the ITRF08 frame, and rates of IGS, we calculate velocities of present-day tectonics in Ninh Thuan and adjacent continental shelf. Daily GPS data with 10° cutting angle was calculated by BERNESE 5.2 software. The free combination of the GPS ionosphere for each point is performed. The latency and slope of the troposphere are estimated randomly at each time interval. Marine loading effects have been modeled. The individual locations have been consolidated into wide solutions. Calculated errors are estimated in the results of GPS handling. Assigning actual error estimates to the coordinates will lead to a more realistic estimate of the uncertainty velocity.

Data from IGS stations were used to calculate present-day velocities in Ninh Thuan and surrounding continental shelf (Table 1-3). The scatter of length, latitude, and height corresponding to the baseline length of each camp are also shown in Figs. 6, 7. The absolute velocity of the network processed is shown in Table 4 and Fig. 8.

Table 1. List of GPS stations used in this study including receiver and antenna type as well as the antenna height

No	Station name	Location	Receiver type/Antenna type	Antenna Height
Large GPS network				
1	CAD1	Ca Du, Khanh Hai, Ninh Thuan	TRIMBLE 4000SSE/TRM22020.00+GP	0.1200 m
2	NHAT	Nha Trang city, Khanh Hoa	TRIMBLE 4000SSI/TRM22020.00+GP	0.1210 m
3	TUYP	Tuy Phong, Binh Thuan	TRIMBLE 4000SSI/TRM22020.00+GP	1.5000 m
4	PQUY	Phu Quy Island, Binh Thuan	TRIMBLE 4000SSI/TRM22020.00+GP	0.1200 m
5	DALA	Da Lat city, Lam Dong	Trimble R7/Trimble Zephyr	1.5045 m
Small GPS network				
1	CAD1	Ca Du, Khanh Hai, Ninh Thuan	TRIMBLE 4000SSE/TRM22020.00+GP	0.1200 m
6	TUT1	Phuoc Dinh	TRIMBLE 4000SSI/TRM22020.00+GP	0.1200 m
7	PMI1	Phuoc Minh	TRIMBLE 4000SSI/TRM22020.00+GP	0.1200 m
8	NPU1	Ninh Phuoc	TRIMBLE 4000SSI/TRM22020.00+GP	0.1200 m
9	NSO1	Ninh Son	TRIMBLE 4000SSI/TRM22020.00+GP	0.1200 m
10	PKA1	Phuoc Khang	TRIMBLE 4000SSI/TRM22020.00+GP	0.1200 m
11	VIS1	Vinh Hy, Vĩnh Hải	TRIMBLE 4000SSI/TRM22020.00+GP	0.1200 m
12	THA1	Dinh Ba, My Hoa	TRIMBLE 4000SSI/TRM22020.00+GP	0.1200 m
IGS network				
13	LHAZ	Lhasa, China	TPS E_GGD/ASH701941.B	0.1330 m
14	TCMS	Hsinchu, Taiwan	LEICA RS500/ LEIAT504	0.0000 m
15	PIMO	Quezon, Philippin	ASHTECH UZ-12/ASH701945C_M	0.0792 m
16	NTUS	Singapore	LEICA GRX1200GGPRO/LEIAT504	0.0776 m
17	COCO	Cocos Island, Australia	TRIMBLE NETR8/AOAD/M_T	0.0040 m
18	IISC	Bangalore, Indian	ASHTECH UZ-12/ASH701945E_M	0.0780 m

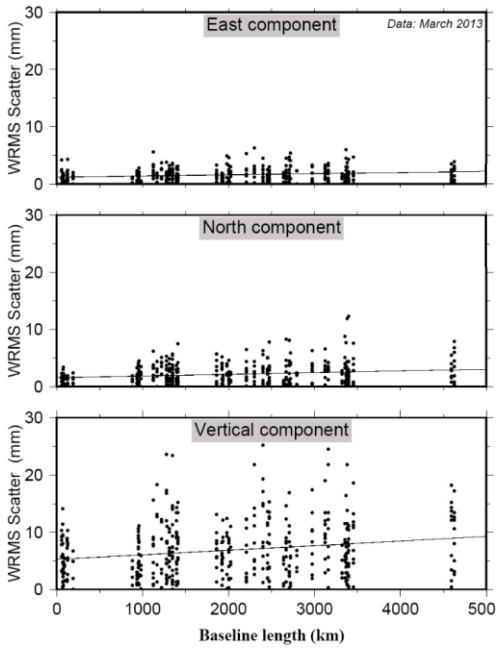

Figure 6. The mean square errors of each component along the side length of the days, in March 2013 campaign of the large GPS network

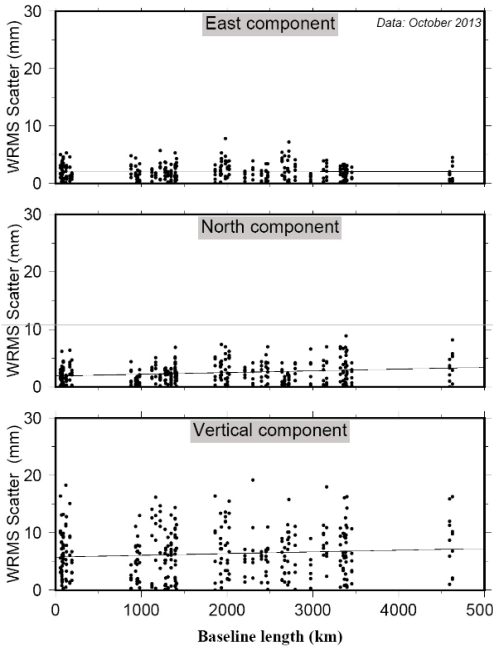

Figure 7. The mean square errors of each component along the side length of the days, in October 2013 campaign of the large GPS network

Table 2. The schedule of GPS campaigns in the small GPS network

No	DOY	CAD	TUT	PMI	NPU	NSO	PKA	VIS	THA
May 2012									
1	129		×						
2	130			×	×				
3	131						×		
4	132							×	
5	133					×			×
6	134	×							
7	135	×		×	×				
8	136	×		×	×	×			
9	137	×			×	×	×		
10	138	×				×	×	×	
11	139	×					×	×	×
12	140	×	×					×	×
13	141	×	×	×					×
14	142		×	×			×		×
15	143		×	×		×		×	
December 2012 and January 2013									
1	364	×	×	×					
2	365	×		×	×				
3	366	×			×	×			
4	001	×				×	×		
5	002	×					×	×	
6	003	×						×	×
7	004	×	×						×
8	005		×		×				×
9	006		×				×		×
10	007			×			×	×	
11	008			×		×		×	
12	009	×			×	×			
September 2013									
1	262	×	×	×	×				
2	263	×		×	×	×			
3	264	×			×	×	×		
4	265	×				×	×	×	
5	266	×					×	×	×
6	267	×	×					×	×
7	268	×	×	×					×
8	269		×	×			×		×
9	270	×			×	×		×	

Table 3. The schedule of GPS campaigns in the large GPS network

No	DOY	CAD1	NHAT	DALA	TUYP	PQUY	CUSV
April 2012							
1	102	×	×	×	×	×	×
2	103	×	×	×	×	×	×
3	104	×	×	×	×	×	×
4	105	×	×	×	×	×	×
5	106	×	×	×	×	×	×
6	107	×	×	×	×	×	×
March 2013							
1	061	×	×		×	×	×
2	062	×	×		×	×	×
3	063	×	×		×	×	×
4	064	×	×		×	×	×
5	065	×	×				×
6	066	×	×				×
7	067	×	×	×			×
8	068	×	×	×			×
9	069	×	×	×			×
10	070	×	×	×			×
October 2013							
1	275	×	×	×	×	×	×
2	276	×	×	×	×	×	×
3	277	×	×	×	×	×	×
4	278	×	×	×	×	×	×
5	279	×	×	×	×	×	×

Table 4. Absolute velocities in ITRF08 from 2012 - 2013 GPS measurements

Unit: mm/year

Station	Lon	Lat	Ve	Vn	Vu	Re	Rn	Ru
NPU1	108,8627	11,4941	22,8	-7,8	-15,7	0,5	0,4	1,7
NSO1	108,8794	11,6397	26,1	-10,0	-34,2	0,6	0,5	2,3
PKA1	109,0236	11,7452	21,4	-0,8	-25,0	0,5	0,4	2,0
PMI1	108,9030	11,4222	26,6	-4,3	-3,4	0,5	0,4	1,8
THA1	109,1602	11,6250	28,5	-5,8	0,9	0,5	0,5	2,2
TUT1	108,9713	11,4672	24,7	-6,3	-16,7	0,5	0,4	1,9
VIS1	109,1963	11,7180	24,8	-8,9	-12,3	0,5	0,4	1,9
CAD1	109,0100	11,6024	23,9	-7,1	-6,3	0,3	0,2	1,1
DALA	108,4456	11,9529	23,2	-4,4	-6,1	0,3	0,3	1,2
NHAT	109,2146	12,2073	24,7	-8,4	-4,7	0,3	0,2	1,1
PQUY	108,9320	10,5163	25,3	-7,4	-3,4	0,3	0,2	1,1
TUYP	108,7151	11,1807	22,5	-7,2	-0,2	0,3	0,2	1,1

Where: Ve - North direction velocity; Vn - North direction velocity, Vu - Vertical direction velocity; Re, Rn and Ru are the errors, respectively (in mm/year)

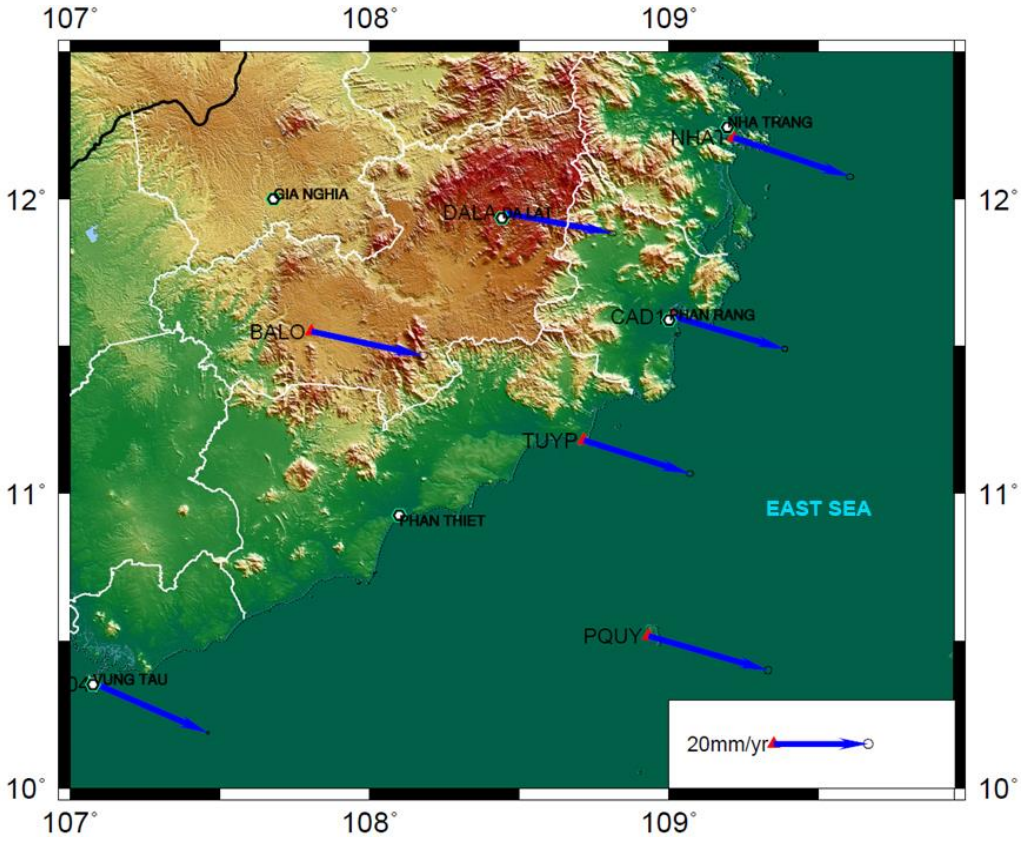

Figure 8. Absolute tectonic velocities of large GPS network determined from three campaign, from March 2012 to October 2013

4.3. Strain rate

From geological observation, geomorphological investigation, and analysis of seismic cross-section at the sea, we mapped capable faults in the Pliocene-Quaternary. Ages of some capable faults have not been determined. However, we accept that these faults activated in the Pliocene. We use the length of capable faults to determine the maximum displacement rate by using the formula of Woodward-Clyde (Woodward-clyde, 1983). Velocities in the fault are maximum at the fault center and minimum at the end of the fault. The tectonic gradient was calculated at the half fault length (Huong et al., 2020). Strain rates vary from 18 to 33 nano/year with an error of 18 nano/yr (Fig. 9).

Based on the reflective seismic cross-section, we map the thickness of Pliocene sediments and then the tectonic gradient. The thickness gradient of the Pliocene sediments is shown in Fig. 10. This value is proportional to the tectonic gradient.

We calculated the present-day velocities and then strain rate. We pay attention not only to the value of the principal strain rate but also to the direction of the principal strain rate. Six triangular subnets are based on GPS stations at Ninh Thuan and the surrounding continental shelf. We set up to calculate the strain rate for each triangle subnet by the least-squares matching method. The maximum principal strain rate, minimum strain rate, maximum shear strain rate, the direction of maximum strain rate, and their

corresponding standard deviation are represented in Table 5. Rotational strain rate, the first and second invariants of the strain rate tensor, and the corresponding deviation for triangle sub-networks are represented in Table 6. The asymmetry of the triangular subnets will affect the accuracy of the calculation. To reduce the deviation related to the asymmetry and form of GPS network, the interpolation is performed by the kriging method at 0.2° × homogeneous mesh nodes. 0.2°. Strain rate parameters are then computed for each 0.2° × 0.2° rectangular subnet. The result of the calculation of the strain rate parameter for rectangular sub-networks from the interpolated velocity in the Ninh Thuan region and surrounding continental shelf are represented in Table 7, Figs. 11, 12.

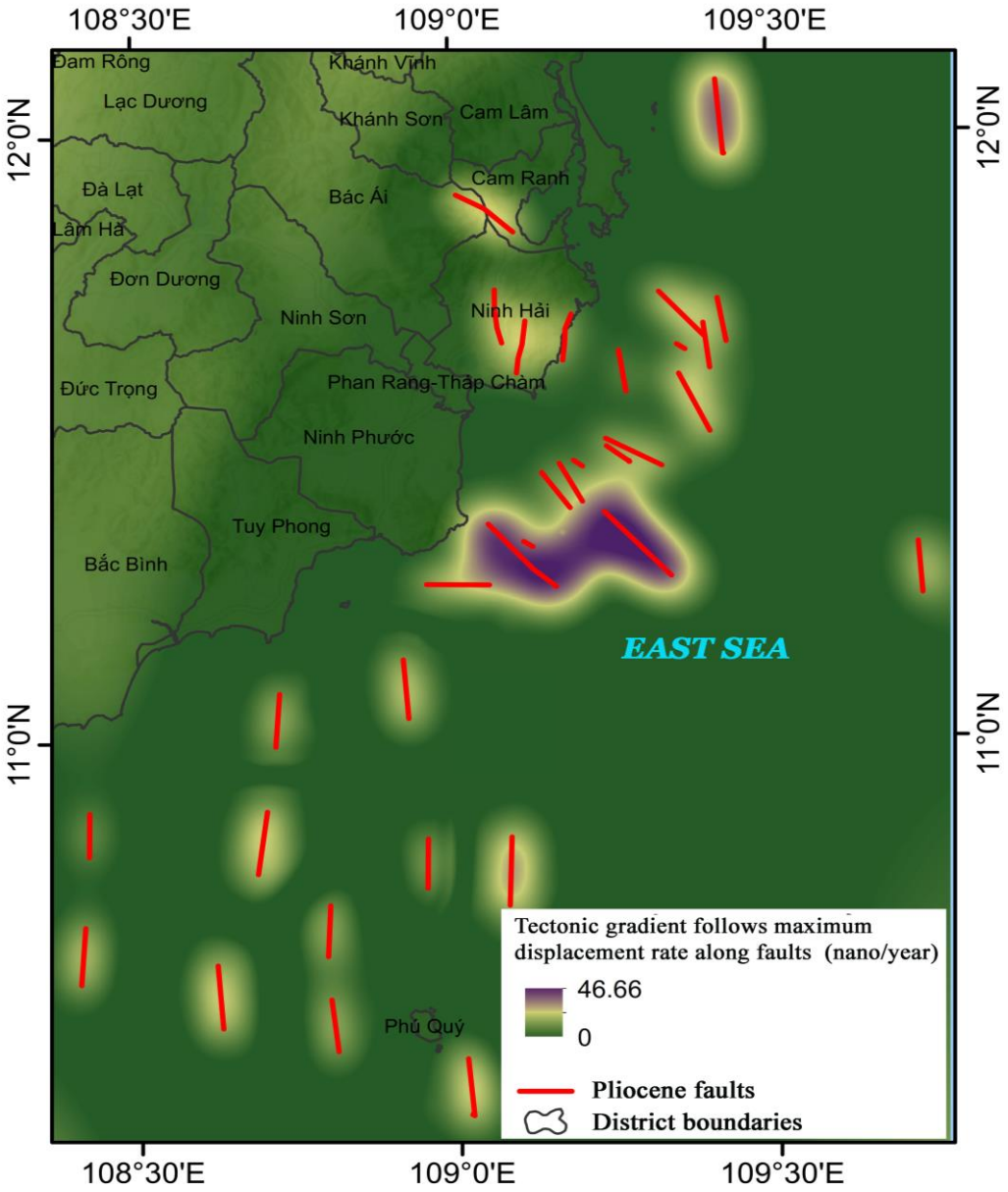

Figure 9. Strain rate determined from capable faults in Ninh Thuan and surrounding regions

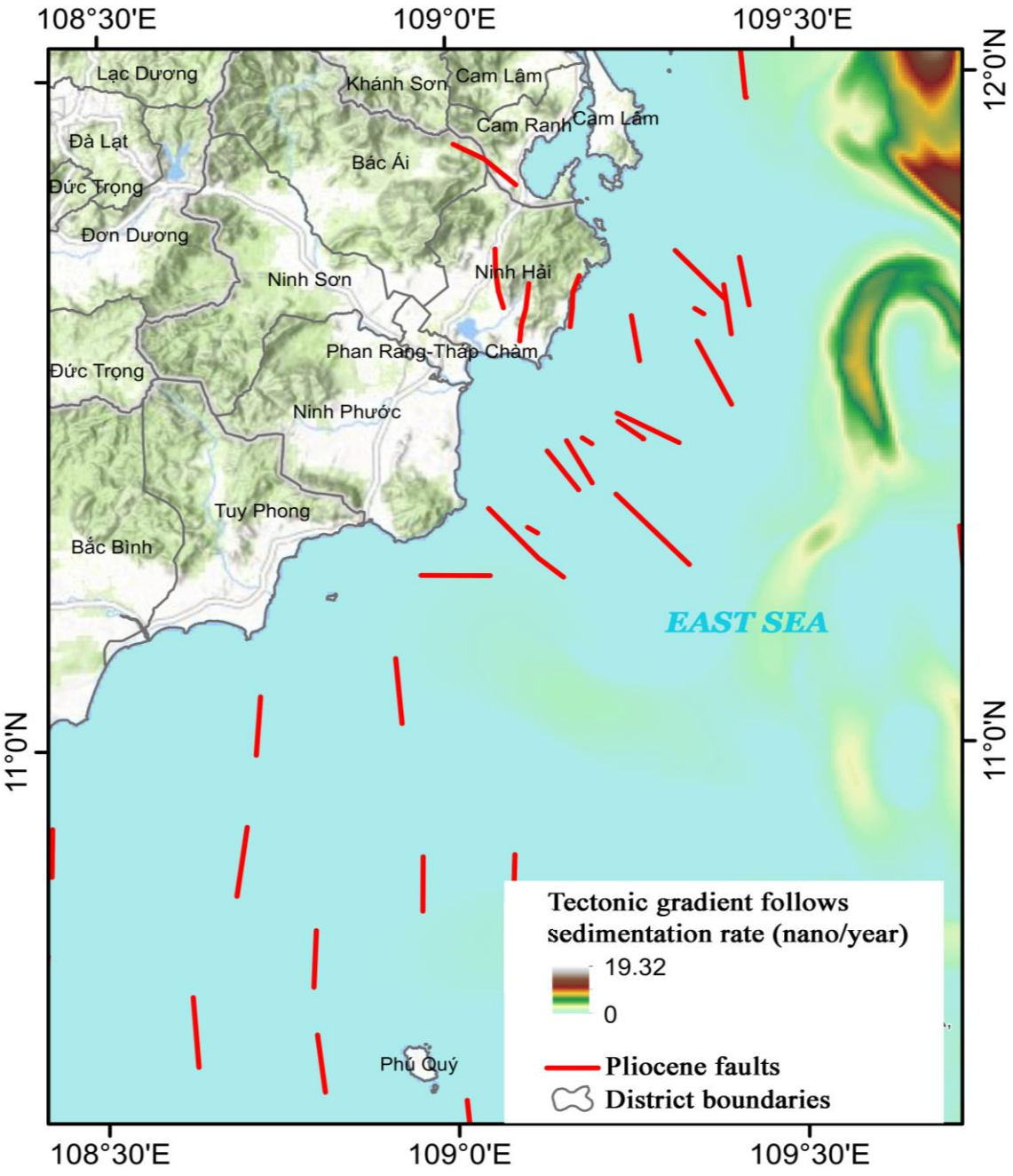

Figure 10. Gradient of Pliocene sediment, proportional to the vertical tectonic gradient on offshore. The values vary from 0 to 20.10^{-9}

Table 5. Principal strain and maximum shear strain rates calculated for triangle sub-networks from the GPS velocities of Ninh Thuan network; planes of maximum shear strain, ψ, occur at 45° to the principal planes, $\psi = \theta \pm 45°$). The maximum shear strain and its planes characterize for the shear strain localization as well as the most potential orientation of strike faulting

Triangle No.	Lon.	Lat.	Maximum Principal strain rate $\dot{\varepsilon}_1$	Standard Deviation of $\dot{\varepsilon}_1$	Minimum Principal strain rate $\dot{\varepsilon}_2$	Standard Deviation of $\dot{\varepsilon}_2$	Maximum shear strain rate $\dot{\gamma}_{max}$	Standard Deviation of $\dot{\gamma}_{max}$	Orientation of maximm Principal strain rate (θ)
	°E	°N	10^{-9}/yr	10^{-9}/yr	10^{-9}/yr	10^{-9}/yr	10^{-9}/yr	10^{-9}/yr	deg
QT04 PQUY TUYP	108.244	10.684	51.2	6.8	24.2	7.3	27.1	10.4	2
QT04 TUYP BALO	107.869	11.029	52.9	5.0	-9.8	13.6	62.7	16.5	131
BALO DALA TUYP	108.323	11.562	39.2	7.3	-4.2	15.4	43.5	16.0	102
TUYP DALA CAD1	108.724	11.579	39.8	7.7	-36.4	22.2	76.2	22.9	95
CAD1 DALA NHAT	108.890	11.921	3.98	7.1	-23.8	15.4	27.8	17.7	101
TUYP PQUY CAD1	108.886	11.099	31.3	4.3	-3.53	38.9	27.1	10.4	92

Table 6. Rotational strain rate, the first and second invariants of the strain rate tensor for triangle sub-networks calculated from the GPS velocities of Ninh Thuan network. Positive values of the first invariant (i.e. 2D dilatational strain) indicate the potential of normal faulting, negative values indicate the potential of reverse faulting. The second invariant (i.e. strain magnidute)

Triangle No.	Lon.	Lat.	Clockwise Rotational strain (CW-SPIN)	Standard Deviation of CW-SPIN	First invariant (Dilatational strain)	Standard Deviation of First invariant	Second invariant (Strain magnitude)
	°E	°N	10^{-9}/yr	10^{-9}/yr	10^{-9}/yr	10^{-9}/yr	10^{-9}/yr
QT04 PQUY TUYP	108.244	10.684	4.1	8.5	37.7	4.9	24.9
QT04 TUYP BALO	107.869	11.029	36.8	7.9	21.6	6.1	16.1
BALO DALA TUYP	108.323	11.562	10.0	8.6	17.5	9.1	9.1
TUYP DALA CAD1	108.724	11.579	1.2	9.2	1.7	12.0	26.9
CAD1 DALA NHAT	108.890	11.921	23.1	9.9	-9.9	8.1	6.9
TUYP PQUY CAD1	108.886	11.099	-15.8	10.2	13.9	19.6	7.4

Table 7. Strain parameters calculated for rectangular sub-networks (0.2° × 0.2°) from the interpolated velocity field of Ninh Thuan network. Standard deviations of the parameters are not shown. Data coverage: 107-110°E, 10-12.5°N

No.	Lon.	Lat.	Principal strain 1	Principal strain 2	Maximum shear strain	Orientation of compressive principal strain	Clockwise Rotational strain	First invariant (Dilatational strain)	Second invariant (Strain magnitude
	°E	°N	10^{-9}/yr	10^{-9}/yr	10^{-9}/yr	deg	10^{-9}/yr	10^{-9}/yr	10^{-9}/yr
1	107.1	10.1	46.1	-0.5	46.6	-10.7	-4.7	22.8	3.4
2	107.3	10.1	53.1	1.5	51.7	-8.2	2.7	27.3	6.2
3	107.5	10.1	54.3	0.7	53.7	-9.6	7.7	27.5	4.3
4	107.7	10.1	53.0	0.4	52.6	-11.1	11.1	26.7	3.2
5	107.9	10.1	50.4	0.2	50.2	-12.5	13.7	25.3	2.4
6	108.1	10.1	47.3	-0.3	47.6	-13.8	15.8	23.5	2.7
7	108.3	10.1	43.9	-1.6	45.5	-15.5	17.6	21.1	5.9
8	108.5	10.1	40.0	-4.2	44.2	-18.2	19.3	17.9	9.2
9	108.7	10.1	34.5	-8.7	43.2	-23.4	20.4	12.9	12.2
10	108.9	10.1	26.4	-14.9	41.3	-32.4	19.3	5.7	14.0
11	109.1	10.1	18.7	-20.3	39.0	-43.1	15.4	-0.8	13.8
12	109.3	10.1	14.1	-21.9	36.0	128.6	11.3	-3.9	12.4
13	109.5	10.1	11.7	-21.2	32.9	122.7	8.4	-4.8	11.1
14	109.7	10.1	10.1	-20.1	30.2	118.4	6.8	-5.0	10.1
15	109.9	10.1	9.0	-19.1	28.1	115.1	5.9	-5.0	9.3
16	107.1	10.3	53.6	-6.6	60.1	-14.4	-3.0	23.5	13.3
17	107.3	10.3	61.3	-1.9	63.2	-10.5	6.3	29.7	7.7
18	107.5	10.3	60.1	-0.7	60.8	-12.0	10.2	29.7	4.6
19	107.7	10.3	56.9	0.8	56.1	-13.4	12.8	28.9	4.8
20	107.9	10.3	53.0	2.0	51.0	-14.2	14.7	27.5	7.2
21	108.1	10.3	48.9	2.6	46.3	-14.6	16.2	25.7	7.9
22	108.3	10.3	45.1	2.4	42.7	-14.8	17.4	23.8	7.4
23	108.5	10.3	41.8	0.9	41.0	-15.8	18.8	21.3	4.2
24	108.7	10.3	37.9	-3.8	41.7	-19.8	21.0	17.1	8.5
25	108.9	10.3	27.1	-13.6	40.7	-32.9	20.0	6.8	13.6
26	109.1	10.3	16.7	-25.0	41.7	129.1	12.9	-4.2	14.4
27	109.3	10.3	13.3	-24.1	37.4	120.2	7.5	-5.4	12.7
28	109.5	10.3	11.7	-22.1	33.8	115.2	5.2	-5.2	11.4
29	109.7	10.3	10.7	-20.4	31.1	112.0	4.4	-4.9	10.4
30	109.9	10.3	9.7	-19.2	28.9	109.7	4.1	-4.8	9.6
31	107.1	10.5	64.0	-22.3	86.3	-18.5	2.5	20.8	26.7
32	107.3	10.5	68.1	-10.9	79.0	-15.7	10.1	28.6	19.3
33	107.5	10.5	64.9	-3.1	68.0	-16.3	12.4	30.9	10.0
34	107.7	10.5	59.8	1.2	58.6	-17.0	14.4	30.5	5.9
35	107.9	10.5	54.0	4.0	50.0	-17.4	15.6	29.0	10.4

36	108.1	10.5	48.3	6.2	42.1	-16.8	16.1	27.3	12.2
37	108.3	10.5	43.4	7.9	35.5	-14.9	15.9	25.7	13.1
38	108.5	10.5	39.8	9.0	30.7	-11.8	15.3	24.4	13.4
39	108.7	10.5	36.5	9.2	27.3	-9.6	14.5	22.9	13.0
40	108.9	10.5	20.3	4.3	16.0	-35.2	9.7	12.3	6.6
41	109.1	10.5	15.1	-21.4	36.5	111.4	1.9	-3.2	12.7
42	109.3	10.5	14.3	-22.6	36.8	107.8	0.6	-4.2	12.7
43	109.5	10.5	13.2	-20.9	34.1	106.1	1.0	-3.9	11.7
44	109.7	10.5	12.0	-19.5	31.5	104.9	1.7	-3.8	10.8
45	109.9	10.5	10.8	-18.5	29.3	104.1	2.3	-3.9	10.0
46	107.1	10.7	73.8	-18.9	92.7	-22.4	2.4	27.4	26.4
47	107.3	10.7	73.6	-10.2	83.8	-21.3	9.5	31.7	19.4
48	107.5	10.7	69.0	-2.8	71.7	-21.4	13.5	33.1	9.8
49	107.7	10.7	61.9	2.3	59.6	-22.0	15.7	32.1	8.5
50	107.9	10.7	53.8	6.1	47.7	-22.6	16.4	30.0	12.9
51	108.1	10.7	45.7	9.8	35.9	-22.2	15.8	27.7	15.0
52	108.3	10.7	38.1	13.6	24.6	-19.0	14.0	25.8	16.1
53	108.5	10.7	32.1	17.1	15.0	-8.3	10.6	24.6	16.6
54	108.7	10.7	29.2	18.8	10.4	23.2	4.3	24.0	16.6
55	108.9	10.7	26.0	8.3	17.7	69.9	-4.8	17.1	10.4
56	109.1	10.7	22.7	-13.9	36.6	89.3	-9.1	4.4	12.6
57	109.3	10.7	18.9	-17.8	36.7	94.8	-5.4	0.5	13.0
58	109.5	10.7	16.2	-17.8	34.1	96.9	-2.5	-0.8	12.0
59	109.7	10.7	14.1	-17.3	31.4	97.9	-0.5	-1.6	11.0
60	109.9	10.7	12.2	-16.9	29.1	98.6	1.0	-2.3	10.2
61	107.1	10.9	83.9	-11.2	95.1	-26.7	3.2	36.4	21.7
62	107.3	10.9	80.5	-5.2	85.7	-26.4	9.8	37.7	14.5
63	107.5	10.9	73.5	0.2	73.3	-26.7	14.8	36.9	2.9
64	107.7	10.9	64.0	4.1	59.9	-28.0	17.4	34.1	11.5
65	107.9	10.9	53.5	7.4	46.1	-30.3	17.6	30.4	14.0
66	108.1	10.9	42.7	11.4	31.3	-33.4	16.0	27.1	15.6
67	108.3	10.9	32.2	16.4	15.8	-37.9	13.0	24.3	16.2
68	108.5	10.9	23.3	20.2	3.1	105.5	8.3	21.7	15.3
69	108.7	10.9	25.7	12.8	13.0	71.2	0.7	19.2	12.8
70	108.9	10.9	27.9	2.5	25.3	77.8	-6.9	15.2	6.0
71	109.1	10.9	27.3	-7.9	35.2	83.2	-9.1	9.7	10.4
72	109.3	10.9	23.7	-12.5	36.1	86.7	-6.9	5.6	12.2
73	109.5	10.9	19.7	-13.7	33.4	89.5	-3.8	3.0	11.6
74	109.7	10.9	16.3	-14.2	30.5	91.8	-1.2	1.0	10.8
75	109.9	10.9	13.6	-14.7	28.3	93.6	0.6	-0.5	10.0
76	107.1	11.1	93.0	-3.5	96.5	-30.7	4.4	44.7	12.8
77	107.3	11.1	88.5	1.2	87.3	-30.9	10.8	44.8	7.2

78	107.5	11.1	79.1	5.0	74.1	-31.9	17.1	42.0	14.0
79	107.7	11.1	66.7	6.1	60.7	-34.3	20.4	36.4	14.2
80	107.9	11.1	54.4	6.2	48.2	-39.5	19.4	30.3	12.9
81	108.1	11.1	43.0	8.2	34.8	131.6	16.7	25.6	13.3
82	108.3	11.1	33.8	10.3	23.6	115.4	13.3	22.1	13.2
83	108.5	11.1	29.8	7.5	22.3	92.6	8.8	18.6	10.6
84	108.7	11.1	30.0	1.8	28.2	84.3	0.4	15.9	5.2
85	108.9	11.1	31.6	-2.5	34.0	83.9	-7.6	14.5	6.2
86	109.1	11.1	31.7	-6.1	37.8	81.2	-7.9	12.8	9.9
87	109.3	11.1	27.5	-8.1	35.6	81.4	-5.5	9.7	10.5
88	109.5	11.1	22.2	-9.5	31.7	83.7	-2.6	6.3	10.3
89	109.7	11.1	17.7	-10.9	28.6	86.7	-0.4	3.4	9.8
90	109.9	11.1	14.4	-12.2	26.7	89.5	1.2	1.1	9.4
91	107.1	11.3	101.0	2.4	99.1	-33.3	3.4	52.0	11.1
92	107.3	11.3	98.0	8.0	90.0	-34.9	10.7	53.0	19.8
93	107.5	11.3	86.5	12.2	74.3	-37.1	20.1	49.3	23.0
94	107.7	11.3	69.6	9.8	59.8	-40.4	25.9	39.7	18.5
95	107.9	11.3	57.6	1.3	56.4	131.6	21.4	29.4	6.0
96	108.1	11.3	47.6	-0.1	47.7	120.1	17.6	23.7	1.7
97	108.3	11.3	40.5	-1.3	41.8	106.3	14.4	19.6	5.2
98	108.5	11.3	39.2	-5.5	44.6	94.2	10.0	16.9	10.3
99	108.7	11.3	41.2	-9.8	51.0	89.5	1.6	15.7	14.2
100	108.9	11.3	40.2	-9.9	50.1	86.5	-6.3	15.2	14.1
101	109.1	11.3	36.2	-5.4	41.6	78.8	-5.0	15.4	9.8
102	109.3	11.3	29.5	-4.1	33.6	76.4	-1.7	12.7	7.8
103	109.5	11.3	22.5	-5.7	28.2	79.1	0.5	8.4	8.0
104	109.7	11.3	17.5	-7.9	25.4	83.1	1.9	4.8	8.3
105	109.9	11.3	14.1	-10.0	24.2	86.7	2.8	2.1	8.4
106	107.1	11.5	111.0	5.8	105.0	-34.6	-0.9	58.3	18.0
107	107.3	11.5	111.0	13.7	96.9	-38.2	7.1	62.2	27.6
108	107.5	11.5	100.0	22.4	78.1	-44.3	20.2	61.4	33.5
109	107.7	11.5	78.9	22.1	56.8	126.6	33.0	50.5	29.5
110	107.9	11.5	69.4	-1.8	71.3	119.3	23.0	33.8	8.0
111	108.1	11.5	55.8	-8.8	64.6	110.2	20.1	23.5	15.6
112	108.3	11.5	44.8	-13.0	57.8	101.9	16.8	15.9	17.1
113	108.5	11.5	39.6	-16.9	56.5	95.7	11.9	11.4	18.3
114	108.7	11.5	37.4	-20.9	58.3	92.9	5.0	8.3	19.8
115	108.9	11.5	38.0	-22.9	60.9	88.8	-4.1	7.6	20.9
116	109.1	11.5	36.4	-1.5	37.9	72.1	2.1	17.5	5.2
117	109.3	11.5	25.5	-0.3	25.8	71.9	5.3	12.6	2.0
118	109.5	11.5	19.1	-2.8	21.9	76.5	5.3	8.1	5.2
119	109.7	11.5	15.2	-5.8	20.9	81.6	5.0	4.7	6.6

120	109.9	11.5	12.6	-8.5	21.1	85.6	4.8	2.1	7.3
121	107.1	11.7	119.0	5.4	113.0	-34.1	-8.2	62.0	18.0
122	107.3	11.7	124.0	13.6	110.0	-38.6	-2.5	68.6	29.0
123	107.5	11.7	124.0	26.0	97.7	131.4	11.0	74.9	40.1
124	107.7	11.7	110.0	28.2	82.1	110.6	33.8	69.3	39.4
125	107.9	11.7	90.0	-0.9	90.9	102.8	32.5	44.5	6.5
126	108.1	11.7	57.6	-16.1	73.7	100.6	27.3	20.8	21.5
127	108.3	11.7	40.6	-23.4	64.0	97.8	20.8	8.6	21.8
128	108.5	11.7	32.1	-24.0	56.1	95.7	16.3	4.0	19.6
129	108.7	11.7	25.2	-26.4	51.5	97.4	13.2	-0.6	18.2
130	108.9	11.7	16.6	-29.7	46.3	104.1	13.4	-6.5	15.7
131	109.1	11.7	9.8	-0.8	10.6	100.5	19.5	4.5	2.0
132	109.3	11.7	12.4	0.6	11.7	77.9	13.6	6.5	2.0
133	109.5	11.7	12.2	-2.1	14.3	79.8	10.0	5.0	3.6
134	109.7	11.7	11.2	-5.1	16.3	83.8	8.0	3.0	5.4
135	109.9	11.7	10.2	-8.0	18.2	86.7	6.9	1.1	6.4
136	107.1	11.9	118.0	0.7	118.0	-31.2	-15.8	59.5	6.3
137	107.3	11.9	124.0	2.6	122.0	-33.4	-16.1	63.5	12.7
138	107.5	11.9	134.0	11.2	123.0	-41.1	-10.8	72.7	27.4
139	107.7	11.9	88.0	22.5	65.5	113.2	31.4	55.2	31.5
140	107.9	11.9	55.4	-8.4	63.8	88.6	48.0	23.5	15.3
141	108.1	11.9	31.2	-22.6	53.9	92.5	35.0	4.3	18.8
142	108.3	11.9	22.0	-31.8	53.8	96.3	25.2	-4.9	18.7
143	108.5	11.9	17.0	-26.5	43.4	97.1	22.2	-4.8	15.0
144	108.7	11.9	12.2	-26.2	38.4	101.2	20.8	-7.0	12.6
145	108.9	11.9	7.6	-24.8	32.4	105.7	20.3	-8.6	9.7
146	109.1	11.9	4.0	-13.3	17.3	106.9	20.1	-4.7	5.2
147	109.3	11.9	4.3	-5.3	9.6	100.3	16.2	-0.5	3.4
148	109.5	11.9	6.3	-4.4	10.7	92.6	12.3	0.9	3.7
149	109.7	11.9	7.5	-6.4	13.8	90.3	9.9	0.6	4.9
150	109.9	11.9	7.8	-8.7	16.5	89.8	8.4	-0.5	5.8
151	107.1	12.1	107.0	-5.8	113.0	-25.8	-20.2	50.8	17.6
152	107.3	12.1	107.0	-16.6	124.0	-23.3	-24.8	45.2	29.8
153	107.5	12.1	95.8	-39.5	135.0	-18.5	-29.6	28.2	43.5
154	107.7	12.1	34.1	-43.3	77.4	0.6	9.4	-4.6	27.2
155	107.9	12.1	2.7	-38.1	40.8	29.5	37.3	-17.7	7.1
156	108.1	12.1	-11.5	-23.7	12.2	74.6	32.9	-17.6	11.7
157	108.3	12.1	-5.0	-33.9	28.9	105.1	27.8	-19.5	9.2
158	108.5	12.1	-0.5	-30.8	30.3	108.9	26.7	-15.6	2.8
159	108.7	12.1	1.8	-28.4	30.2	107.3	24.2	-13.3	5.1
160	108.9	12.1	1.7	-26.2	27.9	105.7	22.2	-12.2	4.8
161	109.1	12.1	-0.3	-20.4	20.1	102.0	20.0	-10.3	1.8

162	109.3	12.1	1.7	-11.2	12.9	109.2	14.9	-4.7	3.1
163	109.5	12.1	4.3	-8.7	13.0	103.5	12.7	-2.2	4.3
164	109.7	12.1	5.5	-9.1	14.6	96.9	10.8	-1.8	5.0
165	109.9	12.1	6.0	-10.5	16.5	93.1	9.2	-2.3	5.6
166	107.1	12.3	91.8	-8.7	101.0	-19.2	-20.3	41.5	20.0
167	107.3	12.3	88.2	-25.0	113.0	-13.9	-22.5	31.6	33.2
168	107.5	12.3	74.1	-49.3	123.0	-7.0	-17.8	12.4	42.7
169	107.7	12.3	43.4	-68.5	112.0	3.2	4.9	-12.5	38.6
170	107.9	12.3	9.6	-64.3	73.9	8.7	22.1	-27.4	17.5
171	108.1	12.3	-16.3	-41.6	25.2	-2.6	21.3	-28.9	18.4
172	108.3	12.3	-17.0	-33.4	16.4	127.8	20.3	-25.2	16.8
173	108.5	12.3	-8.1	-33.4	25.3	114.4	20.9	-20.8	11.6
174	108.7	12.3	-3.1	-31.3	28.2	109.1	21.1	-17.2	7.0
175	108.9	12.3	-0.1	-28.7	28.6	105.2	20.7	-14.4	1.4
176	109.1	12.3	3.2	-25.1	28.3	103.0	20.5	-10.9	6.4
177	109.3	12.3	6.2	-16.9	23.1	108.7	16.1	-5.4	7.2
178	109.5	12.3	5.0	-13.4	18.4	104.9	12.9	-4.2	5.8
179	109.7	12.3	4.7	-12.5	17.2	98.9	10.9	-3.9	5.4
180	109.9	12.3	4.8	-12.8	17.6	94.4	9.3	-4.0	5.6
181	107.1	12.5	77.8	-6.1	83.9	-12.1	-18.7	35.9	15.4
182	107.3	12.5	75.7	-19.6	95.3	-5.7	-17.6	28.1	27.2
183	107.5	12.5	68.6	-36.8	105.0	1.4	-9.4	15.9	35.5
184	107.7	12.5	55.6	-55.2	111.0	7.8	7.9	0.2	39.2
185	107.9	12.5	23.9	-59.7	83.6	5.6	13.7	-17.9	26.7
186	108.1	12.5	-8.3	-46.0	37.6	-16.4	4.0	-27.1	13.8
187	108.3	12.5	-12.8	-31.9	19.1	133.9	8.3	-22.3	14.3
188	108.5	12.5	-8.1	-31.7	23.6	113.9	12.6	-19.9	11.4
189	108.7	12.5	-4.0	-31.3	27.2	106.6	15.1	-17.6	8.0
190	108.9	12.5	-0.7	-29.4	28.6	103.0	16.3	-15.0	3.3
191	109.1	12.5	2.3	-25.9	28.2	101.9	16.1	-11.8	5.5
192	109.3	12.5	4.2	-20.8	25.0	102.5	14.2	-8.3	6.6
193	109.5	12.5	4.3	-17.2	21.5	100.8	11.9	-6.5	6.1
194	109.7	12.5	4.0	-15.5	19.5	96.9	10.2	-5.8	5.6
195	109.9	12.5	3.9	-15.0	19.0	93.3	8.9	-5.6	5.4

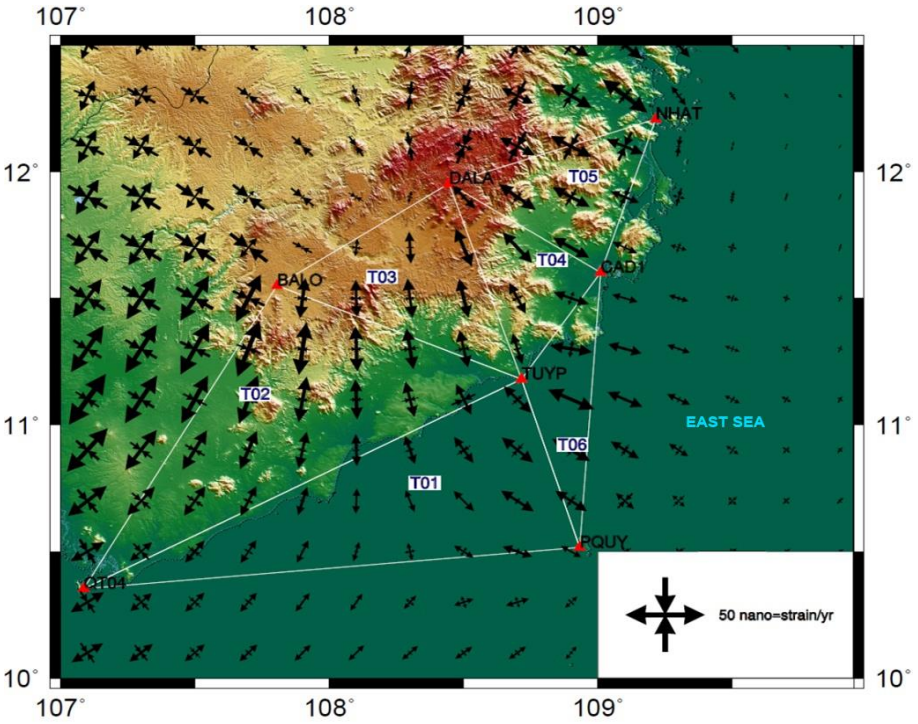

Figure 11. Principal strain rate calculated from present tectonic velocities. Earthquake focal mechanisms indicated that present state of stress is strike-slip regime

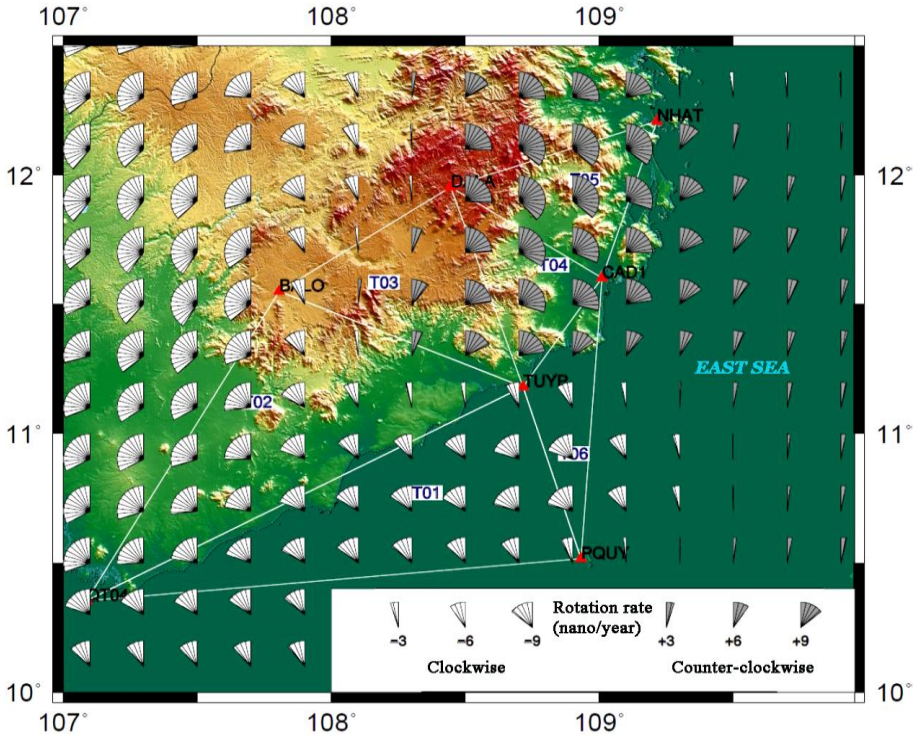

Figure 12. Shear strain rate calculated from present tectonic velocities

5. Discussions

5.1. Present tectonic velocities

The results show that CAD1 moves eastward with a velocity of 23.9 mm/yr, to southward with a velocity of 7.1 mm/yr. The speed of DALA moves to the east with a rate of 23.2 mm/yr, to southward with a rate of 4.4 mm/yr. NHAT moves eastward at a velocity of 24.7 mm/yr. and 8.4 mm/yr southward, respectively. PHUQ moves eastward at 25.3 mm/year and southward with 7.4 mm/yr. TUYP moves eastward with 22.5 mm/yr and southward with 7.2 mm/yr.

Using data from the National Geodesy Bureau, HOCM moves eastward 23.3 mm/year and southward 11.1 mm/yr. QT04 (Vung Tau) moves eastward with a rate of 23.6 mm/yr. and southward with a rate of 11.0 mm/year.

5.2. Strain rate

The first result of the contemporary tectonic gradient in Ninh Thuan and surrounding regions was represented in Trinh et al. (2015). The deformation in the Ninh Thuan region and surrounding continental shelf is dominated by the strike-slip movement from Pliocene to the present day. This means the strain rate of horizontal movement is much higher than the tectonic gradient of vertical movement. The strain rate in Pliocene determined in this study is the same as the strain rate in the late Pleistocene (Huong et al., 2020). The strain rate calculated from velocities of present-day tectonics is in the same value as the strain rate calculated from other data like capable faults, Pleistocene terraces, and the thickness gradient of Pliocene sediments. The low value of strain rate indicates the returned period of the earthquake in this region is long and we have to study late Pliocene tectonics to the current time for the evaluation of seismic hazards. From Pliocene time up to the present day, the deformation in the Ninh Thuan region and surrounding continental shelf is controlled by a strike-slip state of stress. This means the gradient of horizontal movement is much higher than the gradient of vertical movement. Russian consultants have paid special attention to the tectonic gradient and used this value to estimate the maximum credible earthquake in this area. However, the Russian consular estimated tectonic gradients from Pleistocene terraces in a small area. The value of the strain rate of 0.08 nano/year estimated by them is much smaller than the results of our study. We cannot make the evidence of the cause of this difference because the Russian consultants did not explain how they calculated the tectonic gradient and how they estimated the age of the terrain surface.

6. Conclusions

In this paper, we provided the evidence of capable faults in Pliocene - Quaternary on offshore. GPS measurement was effected from 2012-2013 in Ninh Thuan and surrounding regions. GPS method demonstrated an effective tool for evaluation of deformation even short repeat time of measurements. The present-day velocities of tectonic movement are determined in a GPS network with velocities eastward from 23 to 25 mm/year, southward from 4 to 8 mm/year. Latitudinal and longitudinal deviations are between 0.9-1.5 mm/year. The strain rate calculated from different sources like capable faults, Pleistocene terrace, Pliocene sediment thickness, and present-day tectonics is not larger than 30 nano/year. The coastal area in Ninh Thuan and surrounding continental shelf is weakly deformed, demonstrating a stable tectonic setting. That is a reason one has to investigate capable faults in the long period from Pliocene - Quaternary to the present day for assessing seismic hazards as suggested by The IAEA.

Acknowledgments

This article is financed by national project KC.09.22/16-20. PTT thanks also the support of the senior research assistant program (VAST), NVCC 11.01/20-20.

References

Allen C.R., Gillespie A., R. Yuan, Han Sieh, Kerry E., Buchun, Zhang, Chengnan, Zhu, 1984. Red River and associated faults, Yunnan Province, China; Quaternary geology, slip rates, and seismic hazard. GSA Bulletin, 95(6), 686-700.

Binh N.T.T., T. Tokunaga, Neil R. Goulty, Hoang Phuoc Son, Mai Van Binh, 2011. Stress state in the Cuu Long and Nam Con Son basins, offshore Vietnam, Mar. Petr. Geol., 28, 973-979.

Bock Y., L. Prawirodirdjo, J. Genrich, C. Stevens, R. Mccaffrey, C. Subarya, S. Puntodewo, E. Calais, 2003. Crustal motion in Indonesia from Global Positioning System measurements, J. Geophys. Res., 108(B8), 2367. Doi: 10.1029/2001JB000324.

Cong D.C., Feigl K.L., 1999. Geodetic measurement of horizontal strain across the Red River fault near Thac Ba, Vietnam, 1963-1994. Journal of Geodesy, 73(6), 298-310.

Dach R., S. Lutz, P. Walser, P. Fridez, 2015. Bernese GNSS Software Version 5.2. https://core.ac.uk/download/pdf/33089329.pdf.

Dong D., Herring T.A., King R.W., 1998. Estimating regional deformation from a combination of space and terrestrial geodetic data. Journal of Geodesy, 72(4), 200-214.

Feigl K.L., Agnew D.C., Bock Y., Dong D., Donnellan A., Hager B.H., Herring T.A., Jackson D.D., Jordan T.H., King R.W., Larsen S., Larson K.M., Murray M.H., Shen Z., Webb F.H., 1993. Space geodetic measurement of crustal deformation in central and southern California, 1984-1992. J.G.R (1978-2012), 98(B12), 21677-21712.

Feigl K.L., D. Ch. Cong, M. Becker, T.D. To, K. Neumann, N.Q. Xuyen, 2003. Insignificant horizontal strain across the Red River Fault near Thac Ba, Vietnam from GPS measurements 1994-2000, Geophys. Res. Abstr., 5, 04707.

Findlay R., P.T. Trinh, 1997. The structural setting of Song Ma region, Vietnam and the Indochina - South China plate boundary problem. Gondwana Research, 1(1), 11-33.

Findlay R.H., 2018. Geometry, kinematics and regional significance of faulting and related lamprophyric intrusion in the mineralised zone at the Pu Sam Cap complex, Northwest Vietnam. Vietnam J. Earth Sci., 40(4), 320-340.

Fyhn Michael B.W., Boldreel Lars O., Nielsen Lars H., 2009. Geological development of the Central and South Vietnamese margin: Implications for the establishment of the Indochinese escape tectonics and Cenozoic volcanism. Tectonophysics, 478(3-4), 184-214.

Hall R., 2002. Cenozoic geological and plate tectonic evolution of SE Asia and the SW Pacific: computer-based reconstructions, model and animations. J. Asian Earth Sci., 20, 353-431.

Hall R., C.K. Morley, 2004. Sundaland Basins, in Continent-Ocean Interactions Within the East Asian Marginal Seas, Geophys. Monogr. Ser., edited by P. Clift et al., AGU, Washington D.C., 149, 55-85.

Hoan V.T., N.T. Lu, M.V. Rodkin, N. Quang, P.T. Huong, 2018. Seismic activity characteristics in the East Sea area, Vietnam J. Earth Sci., 40(3), 240-252.

Huchon P., X. Le Pichon, C. Rangin, 1994. Indochina peninsula and the collision of India and Eurasia, Geology, 22, 27-30.

Huong N.V., et al., 2020. Recent tectonics, geodynamics and seismotectonics in the Ninh Thuan Nuclear Power plants and surrounding regions, South Vietnam. J. Asian Earth Sci., 187, 10408. https://doi.org/10.1016/j.jseaes.2019.104080.

Huong T.T., Ng. Hoang, 2018. Petrology, geochemistry, and Sr, Nd isotopes of mantle xenolith in Nghia Dan alkaline basalt (West Nghe An): implications for lithospheric mantle characteristics beneath the region. Vietnam J. Earth Sci., 40(3), 207-227.

Iwakuni M., T. Kato, H. Takiguchi, T. Nakaegawa, M. Satomura, 2004. Crustal deformation in Thailand and tectonics of Indochina peninsula as seen from GPS observations, Geophys. Res. Lett., 31, L11612. Doi: 10.1029/2004GL020347.

Japan Atomic Power Company (JAPC), 2013. Ninh Thuan 2 Nuclear Power Plant Project Feasibility Study - Volume 3: Specialized reports of topography, geology and hydrogeology investigation, chapter 2: Geology, 835p.

Kreemer C., Holt W.E., Goes S., Govers R., 2000. Active deformation in eastern Indonesia and the Philippines from GPS and seismicity data. J. G. R., 105, 663-680.

Leloup P., R. Lacassin, P. Tapponnier, U. Scharer, D. Zhong, X. Liu, L. Zhang, S. Ji, P.T. Trinh, 1995. The Ailao Shan-Red River shear zone (Yunnan, China), Tertiary transform boundary of Indochina, Tectonophysics, 251(1-4), 3-84.

Leloup P.H., N. Arnau, R. Lacassin, J.R. Kienast, T.M. Harrison, P.T. Trinh, A. Replumaz, P. Tapponnier, 2001. New constraints on the structure, thermochronology and timing of the Ailao Shan-Red river shear zone, SE Asia, J. G. R., 106, 6657-6671.

Michel G.W., Becker M., Angermann D., Reigber C., Reinhart E., 2000. Crustal motion in E- and SE-Asia from GPS measurements. Earth Planets Space, 52, 713-720.

Michel G.W., Yu Y.Q., Zhu S.Y., Reigber C., Becker M., Reinhart E., Simons W., Ambrosius B., Vigny C., Chamot-Rooke N., Pichon X.L., Morgan P., Matheussen S., 2001. Crustal motion and block behaviour in SE-Asia from GPS measurements. Earth and Planetary Science Letters, 187(3), 239-244.

Morley C.K., Tingay M., Hillis R., King R., 2008. Relationship between structural style, overpressures and modern tress, Baram Delta Province, NW Borneo. J. Geophys. Res., 113, B09410. Doi: 10.1029/2007JB005324.

Nhung B.T., N.H. Phuong, P.T. Truyen, N.T. Nam, 2018. Assessment of earthquake-induced liquefaction hazard in urban areas of Hanoi city using LPI-based method. Vietnam J. Earth Sci. 40(1), 78-96.

Pearson C., Snay R., 2012. Introducing HTDP 3.1 to transform coordinates across time and spatial reference frames. GPS Solution. Doi: 10.1007/s10291-012-0255-y.

Peltzer G., Tapponnier P., 1988. Formation and evolution of strike-slip faults, rifts, and basins during the India-Asia collision: an experimental approach. J.G.R., 93, 15085-15117.

Phuc L.T., Hiroshi Tachihara, Tsutomu Honda, L.T. Tuat, B.V. Thom, N. Hoang, Yuriko Chikano, Katsuji Yoshida, N.T. Tung, P.N. Danh, N.B. Hung, T.M. Duc, P.D.M. Vu, N.T.M. Hoa, H.T. Bien, T.Q. Quy, N.T. Minh, 2018. Geological values of lava caves in Krongno Volcano Geopark, Dak Nong, Vietnam. Vietnam J. Earth Sci., 40(4), 299-319.

Rangin C., Huchon P., Le Pichon X., Bellon H., Lepvrier C., Roques D., Nguyen Dinh H., Phan Quang Q., 1995. Cenozoic deformation of center and south Vietnam. Tectonophys., 251, 176-196.

Replumaz A., Lacassin R., Tapponnier P., Leloup P.H., 2001. Large river offsets and Plio-Quaternary dextral strike-slip rate on the Red River fault (Yunnan, China). Journal of Geophysical Research, 106, 819-836.

Shen Z.K., Lü J., Wang M., Bürgmann R., 2005. Contemporary crustal deformation around the southeast borderland of the Tibetan Plateau. J. G. R. (1978-2012), 110(B11).

Simons W.J.F., Socquet A., Vigny C., Ambrosius B.A.C., Haji Abu S., Promthong C., Subarya C., Sarsito D.A., Matheussen S., Morgan P., Spakman W., 2007. A decade of GPS in Southeast Asia: Resolving Sundaland motion and boundaries. J. G. R. 112(B6). B06420. Doi: 10.1029/2005JB003868.

Tapponnier P., Peltzer G., Armijo R., 1986. On the me, chanics of the collision between India and Asia. In: M.P. Coward and A.C. Ries (Editors), Collision Tectonics. Geol. Soc. Spec. Publ., 19, 115-157.

Tapponnier P., Peltzer G., Le Dain A.Y., Armijo R., Cobbold P., 1982. Propagating extrusion tectonics in Asia: new insights from simple experiments with plasticine. Geology, 10(12), 611-616.

Taylor B., D.E. Hayes, 1980. The tectonic evolution of the South China Basin, in The Tectonic and Geologic Evolution of Southeast Asian Seas and Islands, Part 1, Geophys. Monogr. Set., edited by D. E. Hayes, AGU, Washington D.C., 23, 89-104.

Thanh N.T., P.J. Liu, M.D. Dong, D.H. Nhon, B.V. Dung, P.V. Phach, 2018. Late Pleistocene-Holocene sequence stratigraphy of the subaqueous Red River delta and the adjacent shelf. Vietnam J. Earth Sci., 40(3), 271-288.

Tregoning P., F. Brunner, Y. Bock, S. Puntodewo, R. McCaffrey, J. Genrich, E. Calais, J. Rais, C. Subarya, 1994. First geodetic measurement of

convergence across the Java trench, Geophys. Res. Lett., 21, 2135-2138.

Trinh P.T., 1993. An inverse problem for the determination of the stress tensor from polyphased fault sets and earthquake focal mechanisms, Tectonophysics, 224, 393-411.

Trinh P.T., Liem N.V., N.V. Huong, H.Q. Vinh, B.V. Thom, B.T. Thao, M.T. Tan, Ng. Hoang, 2012. Late Quaternary tectonics and seismotectonics along the Red River fault zone, North Vietnam. Earth-Science Reviews, 114(3), 224-235.

Trinh P.T., N.V. Liem., V.Q. Hai, T.V. Phong, N.V. Huong, N.V. Thuan, N.Q. Xuyen, B.V. Thom, N.D. Tuc, H.Q. Vinh, N.H. Thinh, B.T. Thao, T.Q. Hung, 2015. Present day tectonic gradient in Ninh Thuan and surrounding region. Vietnam Journal of Marine Science and Technology; 15(3), 209-224 (in Vietnamese).

Trinh P.T., Vinh H.Q., Van Huong N., Van Liem N., 2013. Active fault segmentation and seismic hazard in Hoa Binh reservoir, Vietnam. Central European Journal of Geosciences, 5(2), 223-235.

Vietnam Electricity, 2013. Report of Ninh Thuan 1 Nuclear Power Plant Project Feasibility Study. Phase 1 site investigation and survey.

Well D.L., Coppersmith K.J., 1994. New empirical relationship among magnitude, rupture length, rupture width, rupture area and surface displacement. Bulletin of the Seismological Society of America, 84, 974-1002.

Woodward-Clyde Consultants, 1983. Seismic exposure study, offshore, southern California. Report to Texaco USA, New Orleans, 178p.